Available online at www.sciencedirect.com
ScienceDirect
Surface Science 600 (2006) 4517–4526
SURFACE SCIENCE
www.elsevier.com/locate/susc

Depth-dependent fct to fcc strain relaxation in $Co_xNi_{1-x}/Cu_3Au(100)$ alloy films

Bo-Yao Wang [a,b,c], Wen-Chin Lin [a,b], Yu-Wen Liao [a,b], Ker-Jar Song [b], Minn-Tsong Lin [a,b,*]

[a] Department of Physics, National Taiwan University, 1 Sec. 4, Roosevelt Rd., Taipei 10617, Taiwan, ROC
[b] Institute of Atomic and Molecular Sciences Academia Sinica, Taipei 10617, Taiwan, ROC
[c] TIGP, Academia Sinica, Taipei, Taiwan, ROC

Received 18 May 2006; accepted for publication 17 July 2006
Available online 4 August 2006

Abstract

$Co_xNi_{1-x}/Cu_3Au(100)$ with $x \leqslant 11\%$ was prepared at room temperature to study the strain relaxation and their correlation with the spin-reorientation transition. The vertical interlayer distance relaxed from 1.66 Å (fct) to 1.76 Å (fcc) while the thickness increased from 8 ML to 18 ML. Such rapid strain relaxation with thickness was attributed to the larger lattice mismatch between Co_xNi_{1-x} and $Cu_3Au(100)$ ($\eta \sim -6.5\%$). The smooth change for crystalline structure was observed during strain relaxation process in which the crystalline structure seems irrespective of the alloy composition. To explain the strain relaxation, a phenomenological model was proposed. We provide a physical picture that the deeper layers may not relax while the surface layer start to relax. This assumption is based on the several experimental studies. Using the strain averaged from all layers of thin film as the volume strain of magneto-elastic anisotropy energy, the interrelation between strain relaxation and spin reorientation transition can be well described in a Néel type magneto-elastic model.

Keywords: Co; Ni; Alloy; Magnetic ultrathin film; Strain relaxation; Spin-reorientation transition

1. Introduction

In the last decade, Néel type model [1] provided a simple physical picture to describe the thickness dependent spin-reorientation transition (SRT) in magnetic ultrathin film systems. In this model, both the surface and the volume strain will contribute to the magnetic anisotropy energy, which is so-called magneto-elastic anisotropy energy. For example, Fe/Cu(100) [2–5] and $Fe/Cu_3Au(100)$ [5–7] exhibit polar magnetization in the low coverage. As the thickness is thicker, the transition of crystalline structure may cause the easy axis of Fe to align on the longitudinal direction. In case of Ni/Cu(100) [8–14], inverse SRT from longitudinal to polar magnetization direction occurs around 7–10 ML. This is mainly attributed to the accumulation of volume magneto-elastic anisotropy energy with the increasing of thickness. Such a strain-induced polar magnetization will turn to longitudinal direction while the strain starts to relax. Meanwhile, the critical thickness of the second SRT occurs at about 35–70 ML, which were reported from different groups [8–14].

However, the strain relaxation in ultrathin film systems has still been an interesting question. In the past, the theoretical report from Chappert and Bruno [15] suggested a physical picture that the strains of all layers would relax simultaneously as the strain relaxation taking place, and predicted that the strain relaxation would follow the tendency of $\epsilon = \eta(t_r/t)$ rule (ϵ is strain, η is lattice mismatch, t_r is the critical thickness of strain relaxation, and t is the thickness). Although such a relaxation picture [15] was supported from the studies of Fe/Cu(100) [2–5] and $Fe/Cu_3Au(100)$ [5–7], other reports [16–19] did not follow this

* Corresponding author. Address: Department of Physics, National Taiwan University, 1 Sec. 4, Roosevelt Rd., Taipei 10617, Taiwan, ROC.
E-mail address: mtlin@phys.ntu.edu.tw (M.-T. Lin).

0039-6028/$ - see front matter © 2006 Elsevier B.V. All rights reserved.
doi:10.1016/j.susc.2006.07.017

strain relaxation tendency. For example, in the study of surface X-ray on Cu/Ni/Cu/Si(100) [16], the measurement of total strain followed $\epsilon = \eta(t_r/t)^{2/3}$ rule instead of $\epsilon = \eta(t_r/t)$ rule. Recently, the TEM and STM studies of FePd/Pd(100) by Halley et al. [17] provided a lot of information about the strain relaxation in the layers with different depth. In their calculations, by means of the self-energy of each dislocation, the interaction energy between all pairs of dislocation, and the interaction energy between the dislocation and the stressed alloy film, the dislocation (strain) as a function of film depth could be calculated and agree well with the experimental data. In other cases, the direct measurement of stress of thin film was carried out for Fe/W(100) [18], FeMn/Cu(100) [19], and Mn/Cu(100) [20]. Their reports suggested that the thin film would still sustain a residual strain even when the strain relaxation takes place. In other words, the strain of all layers would not totally relax while the strain relaxation of surface layers is observed. Based on these studies, it is possible that in some systems, even when the strain is relaxing on the surface layer, the buried layers remain strained. Since the lattice mismatch of Ni/Cu(100) ($\eta \sim -2.5\%$) is so small that the relaxation process could be changed easily with the condition of preparation, it is difficult to study thickness dependent strain relaxation accurately.

In this work, $Co_xNi_{1-x}/Cu_3Au(100)$ with $x < 11\%$ is prepared at room temperature. The substrate Cu(100) ($a = 3.61$ Å) [3,8] is replaced by $Cu_3Au(100)$ ($a = 3.75$ Å) [21] in order to get the more obvious strain relaxation. The small concentration of Co can provide another point of view for the SRT studying. Due to the similar bulk lattice constants of fcc Co ($a = 3.54$ Å) [8,9] and Ni ($a = 3.52$ Å) [8,9], and the only small concentration of Co, the morphology and crystalline structure seems irrespective of alloy composition. The relaxation process of $Co_xNi_{1-x}/Cu_3Au(100)$ start to occur at about 8 ML. The vertical interlayer distance is increasing smoothly from 1.66 Å (fct) to 1.76 Å (fcc) while the thickness increase from 8 ML to 18 ML. Based on the information about the growth, morphology, and crystalline structure, a detailed investigation about the process of strain relaxation could be achieved. Since the strain relaxation process could not be explained by previous rules ($\epsilon = \eta(t_r/t)$ [15] and $\epsilon = \eta(t_r/t)^{2/3}$ [16]), a surface relaxation model is proposed to describe the thickness dependent strain relaxation. This model suggests that the strain measured from LEED I/V is "surface strain", which is not the same as the strain of the embedded layers. The average strain summed up all layers is more similar to the rule of $\epsilon = \eta(t_r/t)^{2/3}$ that is measured from the surface X-ray [16]. Besides, the more atoms per layer measured from the elongated period of MEED is consistent with the prediction from the model. Although the morphology and crystalline structure seems irrespective of the concentration of Co ($\leqslant 11\%$), the critical thickness for SRT shifted dramatically with the alloy composition. Importantly, using the surface strain and average strain as the parameters, the boundary of SRT can be fitted well from Néel type magneto-elastic model, and the contribution from various kinds of anisotropy energy can be clarified.

2. Experiment

The magnetic ultrathin film was prepared and investigated in situ in ultrahigh vacuum (UHV) chamber with base pressure better than 2×10^{-10} Torr. The UHV system equipped with facilities for spot profile analysis low energy electron diffraction (SPA-LEED), Auger electron spectroscopy (AES), medium energy electron diffraction (MEED), and magneto-optic Kerr effect (MOKE). The scanning tunneling microscope (STM) measurement was carried out in another UHV chamber equipped with the similar facilities as previous one. AES was used to check the surface contamination and alloy composition of the films. The real space morphology of thin film was measured from the STM. The average interlayer distance was estimated by analyzing the LEED I/V curves using the kinematics approximation [9]. MOKE was used to measure the magnetic property of thin films in both longitudinal and polar geometry. The $Cu_3Au(100)$ single crystal with miscut 0.1° was cleaned by cycles of 3 keV Ne ion sputtering. After cleaning, the substrate was annealed at 765 K for 5 min and then at 645 K for 30 min to get surface with large terrace size (~300 nm) and well-ordered C(2 × 2) structure. The ultrathin Co_xNi_{1-x} alloy films were prepared by co-deposition using two evaporators (EFM-3 OMICRON). The growth of these ultrathin films was monitored by MEED with 5 keV beam energy and 1° glancing angle. From the periodicity of the MEED oscillation, the deposition rate was calibrated precisely. Unless explicitly specified, all the films were deposited while the substrate was held at 300 K with a deposition rate around ~80 s/ML. The pressure remains better than 3×10^{-10} Torr during the deposition process.

3. Results

3.1. MEED oscillation

Fig. 1 shows the MEED oscillations of various $Co_xNi_{1-x}/Cu_3Au(100)$ alloy films grown at 300 K. The characteristic feature of all MEED curves (0–11%) are similar. This may result from the similarity of the bulk fcc lattice constant between Co and Ni. These MEED curves all reveal more then 15 oscillations. The periodically of the MEED oscillations also change with thickness even the deposition rate is very stable. The inset of Fig. 1 depicts the period (time intervals between adjoin peaks) as a function of oscillation index. The first two-irregular oscillations may result from the alloying effects between Ni and substrate. After that, the regular periods persist from the third to the fifth oscillations, which reveal layer-by-layer growth mode. Above the fifth oscillation, the periods start to change and the amplitudes are reduced. Within the seventh

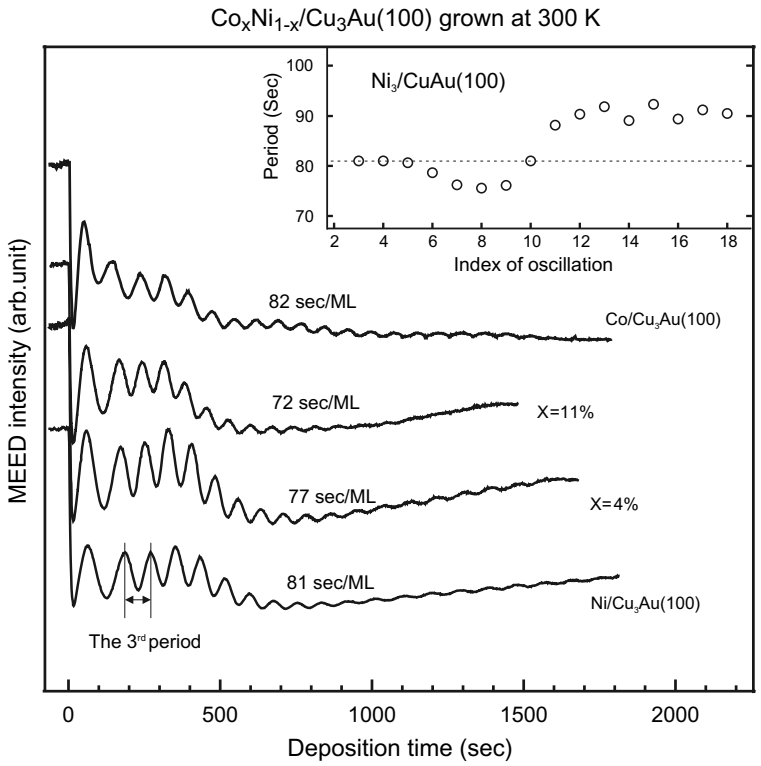

Fig. 1. MEED oscillations of $Co_xNi_{1-x}/Cu_3Au(100)$ alloy films grown at 300 K with various compositions. The curves behavior of alloy films with $x \leqslant 11\%$ seems irrespective of composition. The layer-by-layer growth exhibited from 2 to 5 ML. Above 6 ML, as shown in inset, the period (time interval) within two adjoin peaks changed slightly with the thickness, which may relate to the change of the thin film properties. In each MEED curve, the deposition time per monolayer is defined from the time interval averaged from the third to the fifth oscillations.

and ninth oscillations, the periods are reduced to about 95% of the previous regular period (third to fifth oscillations). After that, the periods start to increase to about 115% of previous regular period. Since the deposition rate was controlled very well by simultaneously monitoring both flux and emission current of EFM3 during deposition. The change of periods in MEED should not be attributed to the unstable deposition rate. Since the variation (<15%) in MEED periods is much larger than the estimation from the simulation, the explanation that irregular MEED period coming from the superposition of periodic function and envelope function is also excluded. As a result, the change of periods with coverage should correspond to the real properties of thin films, both in the growth mode and the morphology.

Compared with the similar studies from other groups, Seider et al. [21] observed only four oscillations, but Braun et al. [22] observed more than 10 oscillations in their system. In our study, the incident angle is another important factor that has great influence on the MEED oscillation. Since the glancing angle in our MEED geometry was about 1°, and the energy of incident electron beam was 5 keV. This geometry may provide the more surface sensitive detection than the conventional MEED geometry (2–3 keV, 3–5°) do. By changing the glancing angle, we can observe similar results as Seider et al. and Braun et al. done. To explain such more oscillations, Braun et al. [22] suggested that the more oscillation was attributed to the stable layer-by-layer growth, which was contributed from the surfactant of gold from substrate. Although we also found a few diffusion of Au atoms from substrate in AES as film grown in room temperature, in advance, we carried out the other comparative experiments of $Ni/Cu_3Au(100)$ with the different growth temperature (350 K and 375 K) and deposition rates (66 s/ML, 43 s/ML, and 23 s/ML), respectively. If the gold atom was a good surfactant of $Ni/Cu_3Au(100)$, we may observe obvious change as we changed the deposition rate or growth temperature. However, no sorely obvious effects were observed in above comparative experiments. So it would still need the more crucial evidences to support that the gold atoms of $Ni/Cu_3Au(100)$ served as a surfactant. Since the regular MEED oscillations in Fig. 1 only appear before the fifth peak, the thickness calibration may be ambiguous in the larger coverage. Therefore, we use the total deposition time over the period averaged from the third to fifth oscillations to mark the thickness of thin films.

3.2. Morphology

Fig. 2(a) shows the SPA-LEED pattern of a clean $Cu_3Au(100)$ substrate which reveals the typical $C(2\times2)$ superstructure. In 3 ML $Ni/Cu_3Au(100)$ as shown in Fig. 2(b), the location of each spot center in reciprocal space is equal to that of substrate, which suggest the growth is coherent. The circle shadow spots represent that

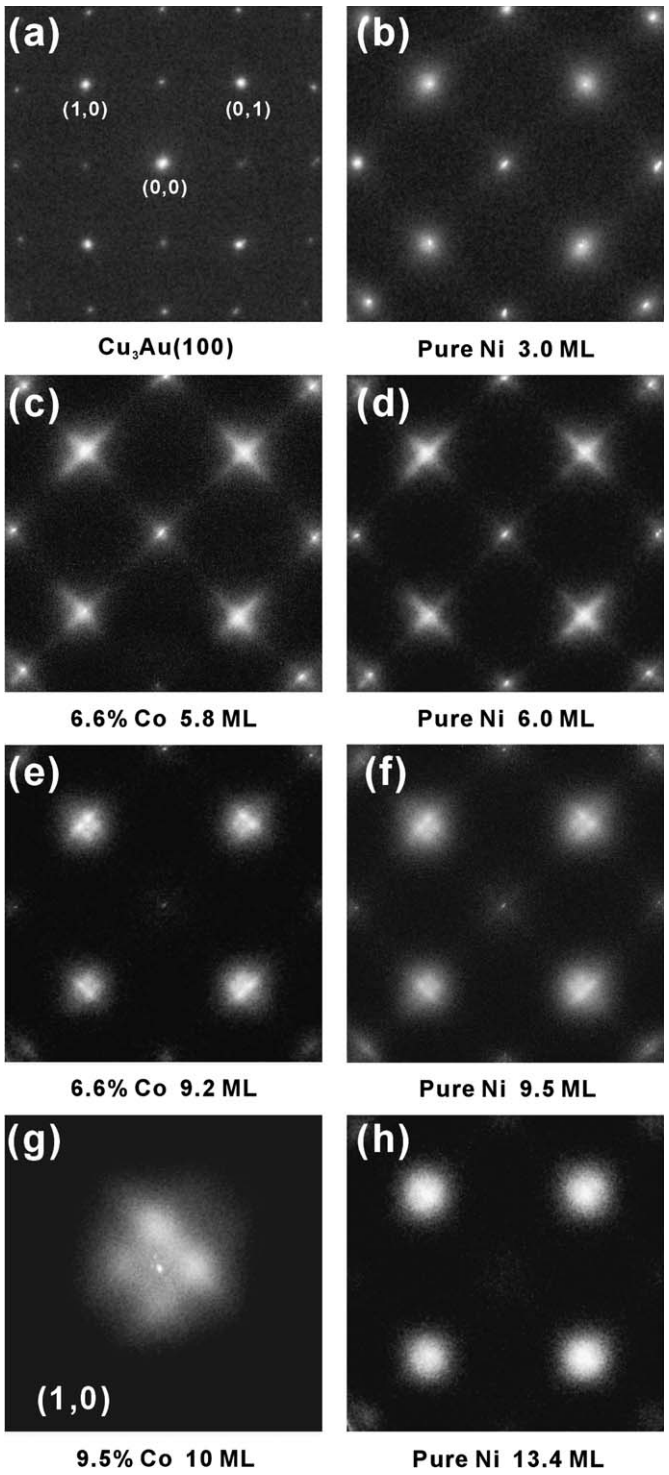

Fig. 2. SPA-LEED patterns of (a) $Cu_3Au(100)$, (b) 3 ML $Ni/Cu_3Au(100)$, (c) 5.8 ML $Co_{0.066}Ni_{0.934}/Cu_3Au(100)$, (d) 6 ML $Ni/Cu_3Au(100)$, (e) 9.2 ML $Co_{0.066}Ni_{0.934}/Cu_3Au(100)$, (f) 9.5 ML $Ni/Cu_3Au(100)$, (g) the (1,0) spot of $Cu_3Au(100)$, and (h) 13.4 ML $Ni/Cu_3Au(100)$, measured at 100 K with beam energy 150 eV.

a few steps formed on surface [23]. The $C(2\times2)$ spots vanished due to the limit of penetration depth of 150 eV electrons or the alloying between Au and Co–Ni (spots vanished up to 1 ML in MEED diffraction pattern). At a thickness of 6 ML, the crossing streaks along [1 1 0] direction are observed (Fig. 2(c) and (d)). Moreover, at thickness ranging from 9 to 11 ML, as shown in Fig. 2(e) and (f), the satellite spots are observed. These distinct satellite spots are observed around the $[0,\pm1]$ and $[\pm1,0]$ beams and are stable when the films are annealed to 400 K. For thickness larger than 12 ML, the satellite spots started to disappear and spots became broad and vague (Fig. 2(h)), and the morphology change slowly with thickness.

Comparing the SPA-LEED patterns of the pure Ni films (Fig. 2(d) and (f)) with the 6.6% Co (Fig. 2(c) and (e)) films, the doping of Co is insignificant to the lateral crystalline structure. This behavior may be ascribed to the similar lattice constants of fcc Co and Ni and only a few doping of Co. The enlarged image of a satellite spot is shown in Fig. 2(g). One possible explanation of the satellite spots might be ascribed to the periodicity of [1 1 0] islands. However, this argument is not consistent with our STM results. Since the satellite spots in SPA-LEED are along [1 0 0] and [0 1 0], which is not the same with the direction of island edges in STM direction. In another possible explanation, the study of MgO/Fe(0 0 1) [24] suggested this kind of the satellite spots may due to the dislocation network while crystalline structure of thin film start to relax. Similar to MgO/Fe(0 0 1), $Ni/Cu_3Au(1\,0\,0)$ is also a strain relaxation system. Since the satellite spots just appear within that range, the explanation of dislocation network may be reliable. However, to explain satellite spots may still need more from the high sensitive experiments and theoretical calculation.

Fig. 3 shows STM images of various $Ni/Cu_3Au(1\,0\,0)$ films with the scale 100 nm × 100 nm. In the first glance, we may see the rectangular islands aligning along [1 1 0] direction in various thicknesses. Actually, similar rectangular islands were also observed in previous STM studies of Ni/Cu(1 0 0) [12,25], Fe/Cu(1 0 0) [14], and $Fe/Cu_3Au(1\,0\,0)$ [5,14]. One possible explanation was given by Shen et al. [12,25] who suggested that the formation of 2-d [1 1 0] rectangular islands was attributed to that the fcc[1 1 0] is the epitaxial direction of fcc [0 0 1] surface. The atoms flowing along [1 1 0] direction could be easier than other directions so as to enhance the formation of [1 1 0] islands. Checking STM images more carefully, 4.5 ML $Ni/Cu_3Au(1\,0\,0)$ (Fig. 3(a)) reveals nearly 2-d islands behavior. As thickness up to 8.5 ML (Fig. 3(b)), the roughness increase obviously. In the 9 and 11 ML film (Fig. 3(c) and (d)), the 3-d islands start to be grown on surface. The STM images show the 2-d to 3-d island growth mode transition with the increasing of thickness. It is possible that the dropping intensity in MEED oscillation and the broader spots in SPA-LEED may be attributed to the formation of the 3-d islands on surface.

3.3. Crystalline structure

Fig. 4 shows the SPA-LEED profiles of various thicknesses from (0,1) to (1,0) spots. The reciprocal spacing

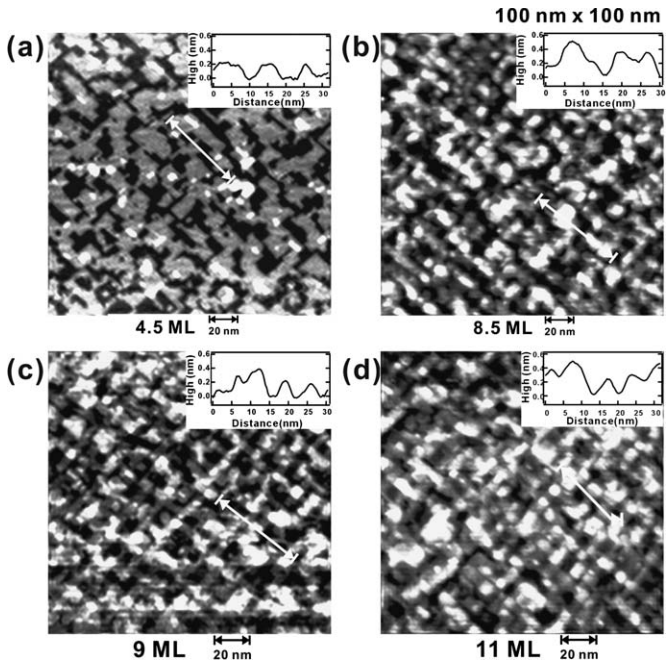

Fig. 3. STM images of 4.5 ML, 8.5 ML, 9 ML, and 11 ML Ni/$Cu_3Au(100)$ films grown and measured at 300 K. The images show the 2-d to 3-d island growth mode transition with the increasing of thickness.

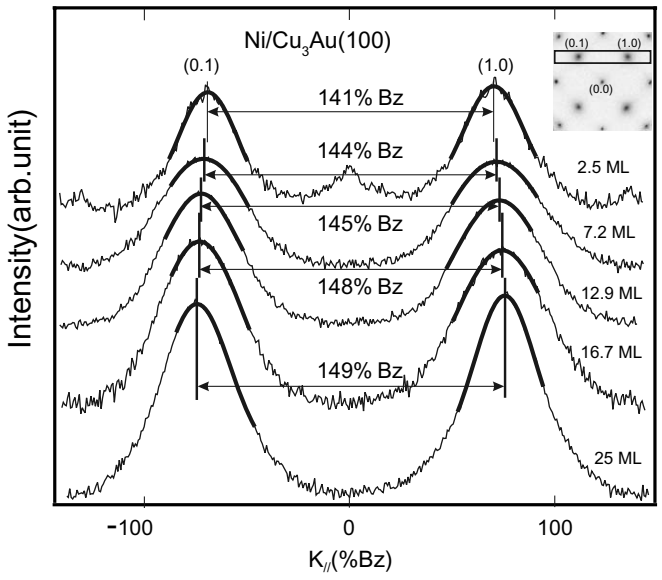

Fig. 4. The SPA-LEED profiles of various Ni/$Cu_3Au(100)$ films with different thickness. The profiles are taken from the integration of a horizontal box including (0, 1) to (1, 0) spot as shown in inset. The distance of $K_{\|}$ between (0, 1) to (1, 0) spots expands with thickness, which indicates the in-plane lattice constant is reduced with thickness.

expands gradually from 141% Bz to 149% Bz when the thickness increases from 2.5 ML to 25 ML. This behavior indicates the in-plane lattice constant reduces gradually from the size of substrate (3.75 Å) to that near the bulk Ni (3.52 Å). Since the volume per unit cell of Co or Ni is smaller than that of $Cu_3Au(100)$ (3.75 Å). Based on the elasticity theory, if the in-plane spacing of Co–Ni is expanded, the vertical interlayer distance would be reduced. This argument was qualitatively consistent with our measurement and will be reported in the following. Fig. 5(a) shows the LEED I/V curve of various thicknesses and alloy composi-

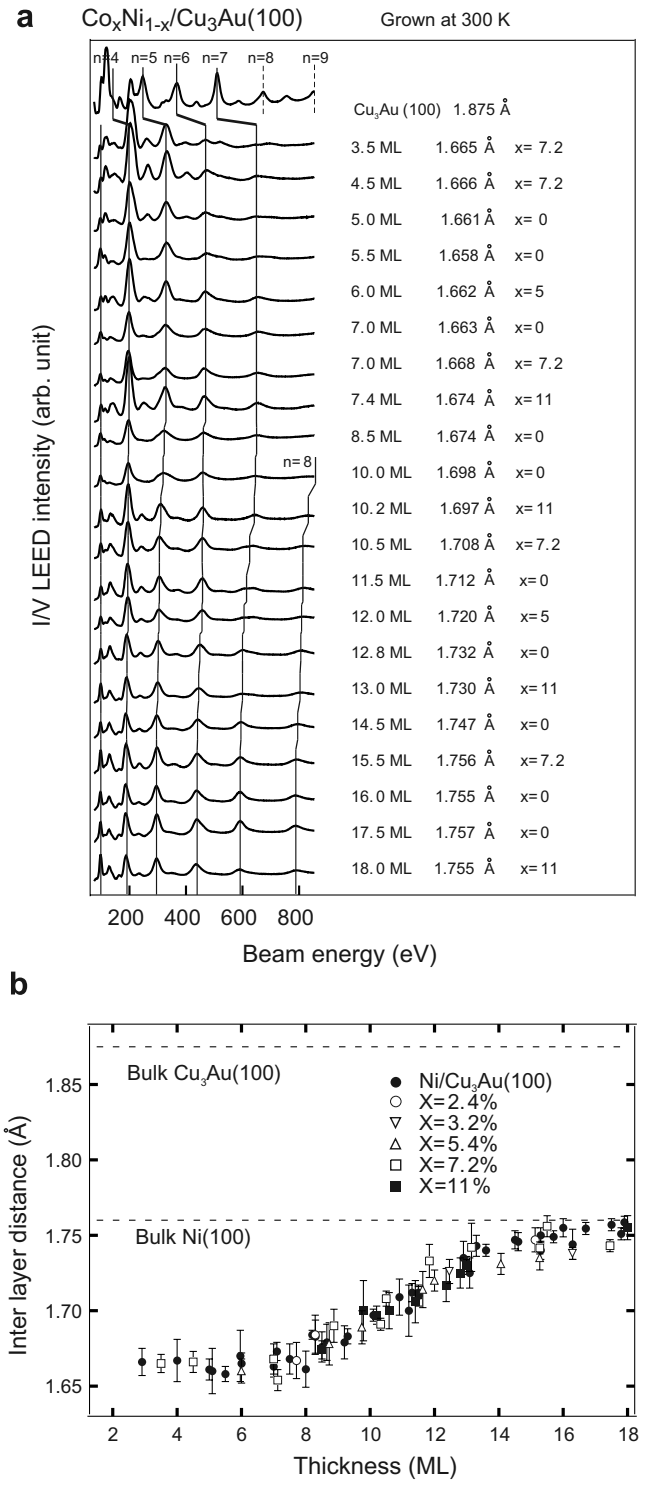

Fig. 5. (a) Intensity vs. (0, 0) beam energy of various Co_xNi_{1-x}/$Cu_3Au(100)$ films, which are grown at 300 K and measured at 100 K. The shift of primary peaks reveals the relative change of the interlayer distances. (b) Average vertical interlayer distances as a function of the thickness, which are fitted from the peaks like (a).

tions as a function of incident beam energy. The peak energy represents the energy of constructive interference in Bragg condition between two layers, and the characteristic interlayer distances can be fitted from the de Brogile relation and the Bragg condition [9]. In Fig. 5(a), the energy of primary peak is shifted with the increasing of thickness, which represents the change of the average interlayer distances. Fig. 5(b) shows the average interlayer distances as a function of thickness. All the lattice constants are fitted from the energy peaks of LEED I/V curves like those in Fig. 5(a). Within 0–7 ML, the average interlayer distances of Co_xNi_{1-x}/$Cu_3Au(100)$ are nearly constant. The interlayer distance clearly increases from 1.66 Å (fct) to 1.76 Å (fcc) when the thickness is increasing from 8 ML to 18 ML. Similar to the result from MEED oscillation, the relaxation of the interlayer distance for alloy films of different alloy composition is indistinguishable. The doping of Co does not result in significant change in the morphology and the crystalline structure. As mentioned above, the distance between (0, 1) and (1, 0) spot in SPA-LEED reveals only small and gradual shift. Besides, the smoothly shifted peaks of LEED I/V curve suggests the structure is changing continuously with the increasing of thickness. Although Co_xNi_{1-x}/$Cu_3Au(100)$ films suffer large strain ($\sim -5.6\%$), the analysis in the above suggests that the structure relaxation near surface is a smooth and continuous process. The gradual strain relaxation in $Co_xNi_{1-x}/Cu_3Au(100)$ could be ascribed to the intrinsic properties of the Ni-like fcc structure. The detail about the strain relaxation will be given in Section 4.

3.4. Spin-reorientation transition

Fig. 6(a) shows the MOKE hysteresis of $Ni/Cu_3Au(100)$ of various thickness. The easy axis switches from longitudinal to polar direction at the thickness about 7.8 ML and switches back at the thickness about 17.2 ML. As the concentration of Co increased to 7.2% (Fig. 6(b)), the polar-oriented magnetization only observed within 9 ML and 13 ML. Moreover, as the Co concentration increased to 11% (Fig. 6(c)), the polar remanence totally disappeared and the easy axis preferred to align longitudinal direction. Since the magnetic moments per unit volume of Co (1.8 μ_b) [26] was nearly three times that of Ni (0.57 μ_b) [26], the Kerr remanence would be enhanced in the films with the larger Co concentration. In our measurement, however, the polar remanences of alloy films were smaller than that of Ni film. A possible explanation might be attributed to the easy axes of alloy films are not exactly along perpendicular direction, and then cause the reduction of polar remanence.

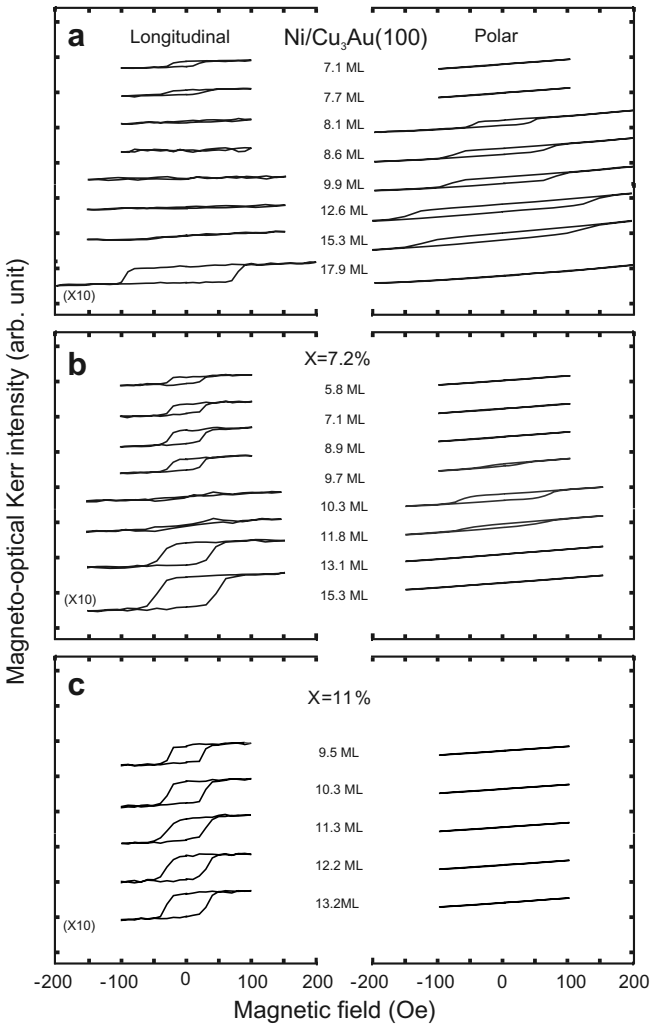

Fig. 6. MOKE hysteresis loops of (a) $Ni/Cu_3Au(100)$, (b) $Co_{0.072}Ni_{0.928}$/$Cu_3Au(100)$, and (c) $Co_{0.11}Ni_{0.89}/Cu_3Au(100)$, which are grown at 300 K and measured at 100 K. The region for polar magnetization reduce with the increasing of Co concentration.

4. Discussion

4.1. Glancing angle dependent MEED oscillations

The MEED oscillations with the incident glancing of 1°, 2°, and 4° are shown in Fig. 7. The behavior of oscillations is strongly influenced by the incident glancing angle. The obvious oscillations do not exhibit in any continuous glancing angle. One possible explanation is attributed to the effect of the out of phase condition of MEED/RHEED, which was reported from Henzler [23]. Conventionally, the roughness effect may cause the minimum (0, 0) beam intensity as films with half filled layers. As a result, the intensity of (0, 0) spot could oscillate until the surface has no roughness contrast. However, if the wave path difference of electron beam between adjoining layers was in phase, the constructive interference between these two reflected electron waves may also enhance the (0, 0) beam intensity as the films are half filled layers. Alternatively, one may choose an out of phase condition to enhance the contrast of oscillation. The out of phase condition in Bragg equation is written as the following:

$$2d\sin\theta = \frac{n\lambda}{2}, \quad n = 1, 3, 5, \ldots, \tag{1}$$

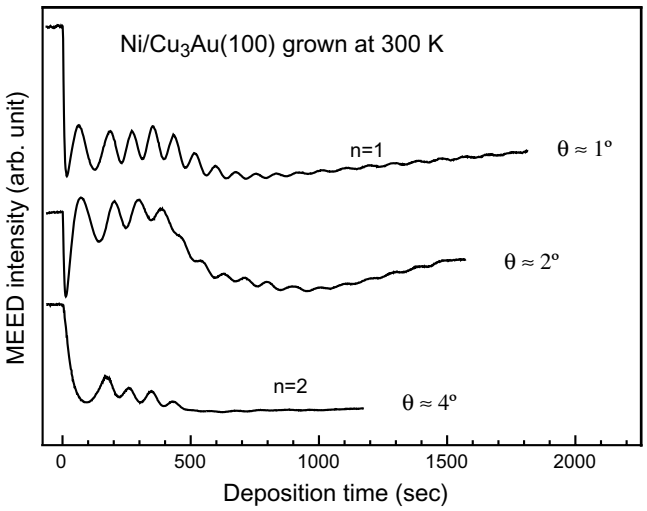

Fig. 7. MEED oscillations of Ni/$Cu_3Au(100)$ grown at 300 K. The incident glancing angles are about 1°, 2°, and 4°. The MEED oscillation observed from Seider et al. is similar to the case with $n = 2$, and that from Braun et al. is similar to the case with $n = 1$.

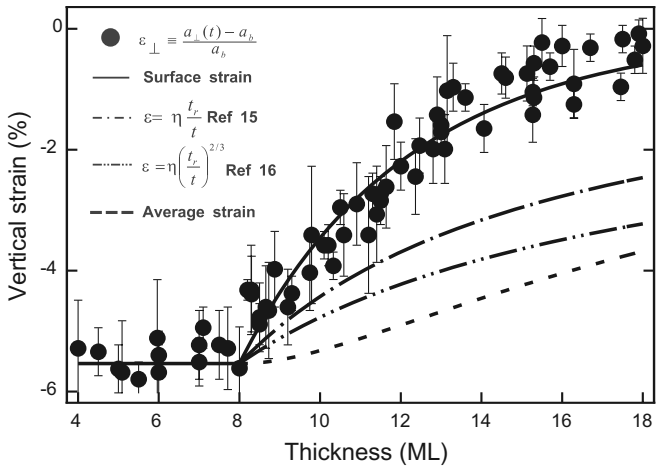

Fig. 8. The strain of $Co_xNi_{1-x}/Cu_3Au(100)$ calculated from LEED I/V as a function of thickness (solid circles). The solid line is the Surface strain fitted from Eq. (12). Line–dash–line shows the strain relaxing with the rule of $\varepsilon = \eta(t_r/t)$. Line–dash–dash–line shows the strain relaxing with the rule of $\varepsilon = \eta(t_r/t)^{2/3}$. The dash line is the average strain, which is calculated from the integration of surface strain equation (13).

where d is the distance between adjoining layers, n are odd numbers. λ can be substituted by the de-Broglie relation, as a result

$$\sin\theta = \frac{n\lambda}{4d} = \frac{nh\lambda}{4d\sqrt{2mE}} \sim 0.025n, \tag{2}$$

where $E = 5$ keV is the electron energy, $d \sim 1.7$ Å is the averaged interlayer distance for $Co_xNi_{1-x}/Cu_3Au(100)$, k is Boltzmann factor, and m is the mass of electron. The first-order condition gives glancing angle $\theta = \arcsin(0.025) \sim 1.53°$, and the second one gives that of $\theta = \arcsin(0.075) \sim 4.3°$. The angle difference between the first-order and the second-order diffraction was about 2.77°, which was qualitatively consistent with the angle difference between the first (~1°) and the third (~4°) MEED oscillation as shown in Fig. 8. The more oscillations will give the more precisely information about the thickness calibration. Compared with the studies from other groups, the MEED oscillation observed from Seider et al. [21] is similar to the case with $n = 2$, and that from Braun et al. [22] is similar to the case with $n = 1$. This estimation not only gives a simple picture for the best condition of glancing angle in MEED oscillation, but also explain why the MEED oscillations are so different from different groups [21,22].

4.2. Strain relaxation model

Conventionally, the strain of ultrathin film is defined as following:

$$\varepsilon_\perp = \frac{a_\perp(t) - a_b}{a_b}, \tag{3}$$

where t is the thickness, a_b is the bulk lattice constant of Ni, and $a_\perp$ is the vertical lattice constant of ultrathin film. If we regard the double interlayer distance given from LEED I/V as the vertical lattice constant, the strain of $Co_xNi_{1-x}/Cu_3Au(100)$ can be calculated as the solid circles shown in Fig. 8. In the past, Chappert and Bruno [15] proposed a strain relaxation picture for ultrathin films and predicted the rule for strain relaxation $\epsilon = \eta(t_r/t)$ (η is lattice mismatch, t_r is the critical thickness of strain relaxation, and t is the thickness). Their model also suggested that individual layers of film will relax simultaneously during strain relaxation, which was supported by the experiments of Fe/Cu(100) [2–5] and Fe/$Cu_3Au(100)$ [5–7]. However, the relaxation process of Cu/Ni/Cu/Si(100) studied by the surface X-ray [16], which revealed $\epsilon = \eta(t_r/t)^{2/3}$ tendency, was also inconsistent with Chappert's prediction. As shown in Fig. 8, the strain relaxation of $Co_xNi_{1-x}/Cu_3Au(100)$ does not follow both the rules $\epsilon = \eta(t_r/t)$ (line–dash–line) and $\epsilon = \eta(t_r/t)^{2/3}$ (line–dash–dash–line). Therefore, constructing a more general model to describe strain relaxation is necessary. Since the strain relaxation is much complicated in the systems with different crystalline structure between film and substrate, we only consider the system that the film and the substrate with similar crystalline structure (i.e. fcc/fcc or bcc/bcc).

Here we consider a thin film system with a lattice mismatch between film and substrate. The lattice mismatch induces the strain relaxation while the coverage is larger than a critical thickness. If such a film is under the layer-by-layer growth mode, due to a coherent growth process, each layer may have the same atom number. If the film start to relax, the atom number of the relaxed layer may be changed. Fig. 9(a) shows the top view of atom with the layer before relaxation. In Fig. 9(b), the density of atoms in one layer is changed after strain relaxation. Since the total area of thin film is not changed, the process of strain relaxation could be simply regarded as the relaxed surface layers are composed of the more or the fewer atoms, which depend on

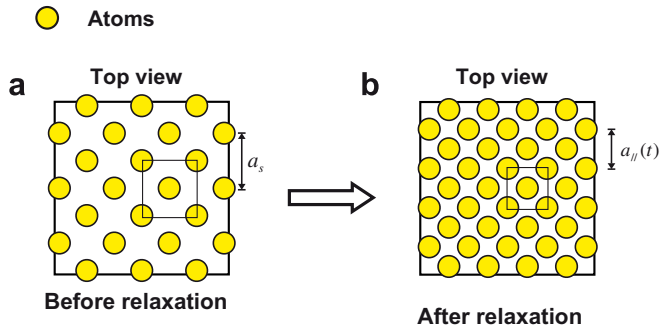

Fig. 9. Illustration of the atoms per layer (a) before the strain relaxation, and (b) under the strain relaxation. The atom number per layer is changed due to the strain relaxation.

the stress direction of thin film. As a result, the average occupied area per two atoms for the case of fcc(100) unit cell can be written as

$$a_{\parallel} = a_s \quad \text{for } t \leqslant t_r, \tag{4}$$

$$a_{\parallel}(t)^2 = \frac{a_s^2 \times \frac{N_0}{2}}{\frac{N_0}{2} + \frac{D(t)}{2}} \quad \text{for } t \geqslant t_r, \tag{5}$$

where t is the thickness, t_r is the critical thickness of strain relaxation. N_0 is the atom number per layer before strain relaxation. a_s is in-plane lattice constant in coherent growth. Since the atom number will change during strain relaxation, here we define $D(t)$ as the excess atom number for individual layer as compared with the atom number of coherent growth layer.

In this relaxation model, we provide a physical picture that the deeper layers may not relax while the surface layer start to relax. This assumption is based on the several experimental studies as following. The studies of TEM in FePd/Pd(100) [17] suggested the dislocation of a relaxed film increases with the depth of film thickness, which means the deeper layers do not relaxed as the top layers start to relax. Besides, the direct measurement of stress of Fe/W(100) [18] also revealed a residual strain even when the thin film under relaxation. Since the crystalline structure for film and substrate are similar in both systems (fcc/fcc for FePd/Pd(100) and bcc/bcc for Fe/W(100)), their results could be reliable for supporting our model.

In Eq. (5), the in-plane lattice constant $a(t)$ depends on the excess atom number $D(t)$. As $t \leqslant t_r$, $a_{\parallel}(t)$ is equal to the in-plane lattice constant of the substrate a_s. As $t \geqslant t_r$, $D(t) < 0$ represents the film is under the compressed strain in in-plane direction (like Pd/Cu_3Au(100) [21]), the surface may be composed of the fewer atoms per layer during strain relaxation. Since the fewer atoms share the same surface area, the in-plane lattice constant will increase. $D(t) > 0$ represents the layer is under the in-plane tensile strain (like Ni/Cu_3Au(100)), the surface layer may be composed of the more atoms per layer during strain relaxation. Since the more atoms share the same surface area, the in-plane lattice constant could be reduced. Moreover, compared with Eqs. (4) and (5), $D(t)$ need to fit with the boundary condition as following:

$$D(t_r) = 0, \tag{6}$$

$$D(\infty) = \frac{N_0(a_s^2 - a_b^2)}{a_b^2}, \tag{7}$$

where a_b is the bulk lattice constant of the film. Eq. (6) represents the excess atom number is zero at $t \leqslant t_r$. Since the layer structure will tend to the bulk structure eventually, $D(\infty)$ should converge to a finite value as shown in Eq. (7), which can be calculated from Eq. (5) by substituting t as t_∞. So if $D(t)$ could be defined, the tendency of in-plane lattice constant could be described. Here we try to solve this problem by analogizing the variation of atom number in each layer as the probability problem. Since $D(t)$ is the excess atom number as compared with the coherent growth, $D(\infty) - D(t)$ could be the allowed unoccupied states for inserting the atom in next layer. It is straight forward to assume that the probability for dislocation or the variation of atom is proportional to the number of unoccupied states. The formula could be written as

$$dD(t) = C * (D(\infty) - D(t))dt. \tag{8}$$

C is a constant to describe the magnitude of the strain relaxation. The C value will relate to how strong of relaxation. Considered the boundary condition, the formula of is solved as

$$D(t) = N_0\eta'[1 - \exp(-C(t - t_r))] \quad \text{for } t \geqslant t_r, \tag{9}$$

$$\eta' \equiv \frac{a_s^2 - a_b^2}{a_b^2}, \tag{10}$$

where C is the only free parameter. The value of η' is a constant, which describes the mismatch of fcc(100) unit area between film and substrate. η' also determines the maximum ratio of available space that the ad atoms could be inserted in. As a result, by substituting $D(t)$ into Eq. (5), the in-plane lattice constant as a function of thickness can be derived. Since the vertical lattice constants have the better contrast than in-plane lattice constant, we choose the vertical strain from experiment to compare that from the strain relaxation model. The vertical strain and in-plane strain could be linked by the constant parameter P, which is so-called Poisson's ratio. Therefore, in-plane and vertical strain as a function of thickness can be written as following:

$$\varepsilon_{\parallel}(t) = \frac{a_{\parallel}(t) - a_b}{a_b} = \frac{a_s}{a_b\sqrt{1 + \eta'[1 - \exp[-C(t - t_r)]]}} - 1, \tag{11}$$

$$\varepsilon_{\perp}(t) = \frac{\varepsilon_{\parallel}(t)}{p} = \frac{1}{p}\left\{\frac{a_s}{a_b\sqrt{1 + \eta'[1 - \exp[-C(t - t_r)]]}} - 1\right\}. \tag{12}$$

The solid line in Fig. 8 is the fitting results from Eq. (12). The tendency agrees well with the strain relaxation from experiment (solid circle). The parameters were obtained from the experiment ($t_r = 8$, $P = -1.18$) or literature ($\eta' = 0.134$, $a_b = 3.52$ Å, $a_s = 3.75$ Å), and $C = 0.23$. Be-

sides, C provides the information that atoms number from a layer to the next layer is increasing with a constant rate of per layer (from Eq. (8)). The larger value of C will means the faster strain relaxation. It is possible that some physical parameters are behind C. However, it still needs the more advanced investigation. Since the strain measured from LEED I/V only represents few surface layers, we regard this strain as the "surface strain". Therefore, the volume strain of thin film could be obtained by averaging and summing over all layers. The average strain as a function of thickness is written as following:

$$\text{Average strain}(t) = \frac{\int_0^t \text{Surface strain}(t)\,\mathrm{d}t}{t}. \quad (13)$$

In Fig. 8, although the relaxation rule $\varepsilon = \eta(t_r/t)^{2/3}$ [13] is not consistent with our surface strain, their rule is qualitatively close to the tendency of average strain we proposed. The possible reason may be attributed to the penetration depth of surface X-ray would be deeper than that of LEED I/V so that their tendency may be close to the average strain which is averaged from all of the layers. As a result, the average strain may be similar to the volume strain in this system. The picture of continuous relaxation may work in the systems with similar structure between film and substrate such as FePd/Pd(100) (fcc/fcc), Ni/Cu(100) (fcc/fcc), $Co_xNi_{1-x}/Cu_3Au(100)$ (fcc/fcc) and Fe/W(100) (bcc/bcc). In these cases, forming the metastable structures like fct and bct may more stable than forming the totally structure transformation.

4.2.1. Correlation MEED oscillation and strain relaxation

Recalling the inset in Fig. 1, MEED curves show the regular oscillation within the third and the fifth peaks. From the seventh to the ninth oscillations, the periods reduced to about 0.95 of previous one. After the ninth peak, the periods gradually increase to about 1.15 times as compared with the third oscillation. This kind of MEED behavior is similar to the report from Braun et al. [22]. A possible explanation for the reduced periods within the seventh and the ninth oscillation was due to the swiftly change of morphology from the flat surface to the island surface. Within the regions of third to fifth oscillations (un-relaxed films) and the 14–17th oscillation (nearly relaxed films), the change of morphology is much insignificant, so the MEED period could roughly be estimated to the time that atoms cover 1 ML on surface. Based on this approximation, the different periodicity for relaxed and un-relaxed films could correspond to the parameter in strain relaxation model. In the model, $N_0 + D(\infty)$ is the atom number in a total relaxed layer. So the value $1 + \eta' = 1.134$ given from $(N_0 + D(\infty))/N_0$ represents the ratio of atoms of surface layer between before and after strain relaxation. This value (1.134) is very close to the ratio of periods in MEED (1.15) between relaxed and un-relaxed films. By this estimation, we could conclude that the MEED oscillation is consistent with the strain relaxation model.

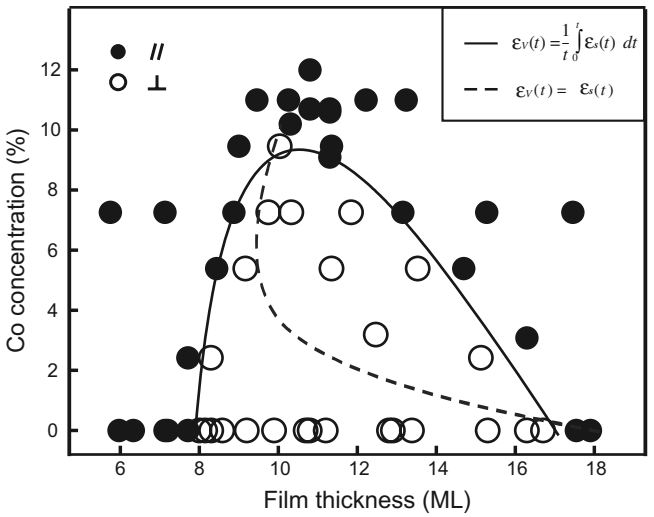

Fig. 10. The SRT phase boundary for $Co_xNi_{1-x}/Cu_3Au(100)$ alloy films measured at 100 K. The solid line is the fitting result from SRT model with the assumption $\varepsilon_v(t) = \frac{1}{t}\int_0^t \varepsilon_s(t)\mathrm{d}t$, in which the SRT model can describe the phase boundary very well. The dash line is the fitting result from the assumption $\varepsilon_s(t) = \varepsilon_v(t)$.

4.2.2. Correlation of spin-reorientation transition and strain relaxation

In SRT system $Co_xNi_{1-x}/Cu(100)$ [8,9], since the strain does not relax within the region of the first SRT boundary, the boundary can be described well by the Néel type model with a constant strain. However, in $Co_xNi_{1-x}/Cu_3Au(100)$, the strain start to relax as $t > 8$ ML. So the strain is not a constant anymore within the range of the first and the second boundaries. So the strain should be regard as a thickness dependent function in strain dependent Néel type model [27]. The SRT phase diagram of $Co_xNi_{1-x}/Cu_3Au(100)$ with various composition and thickness are shown in Fig. 10. Both critical thicknesses of SRT shift obviously with x varying from 0% to 11%. However, if we regard $\varepsilon_s(t) = \varepsilon_v(t)$ in Néel type model, the fitting result just like the dash line as shown in Fig. 10. The tendency of fitting line is totally different with the second SRT boundary. If we treat volume strain as the average of surface strain $\varepsilon_v(t) = \frac{1}{t}\int_0^t \varepsilon_s(t)\mathrm{d}t$, both SRT boundaries of $Co_xNi_{1-x}/Cu_3Au(100)$ can be described very well [27]. So this strain relaxation model not only provides physical picture for strain relaxation but also supports detail strain information to describe the strain dependent SRT behavior.

5. Summary

$Co_xNi_{1-x}/Cu_3Au(100)$ with $x \leqslant 11\%$ revealed a layer-by-layer growth mode up to 5 ML, and the MEED oscillation was strongly influenced by the incident glancing angle. At the thickness about 8 ML, the strain started to relax from fct to fcc. The SRT behavior of $Co_xNi_{1-x}/Cu_3Au(100)$ is significantly influenced by the strain relaxation. To explain the fct to fcc strain relaxation process, a

phenomenological model was proposed. The strain relaxation is correlated to the variation of atom number in individual layer. In this relaxation model, we provide a physical picture that the deeper layers may not relax while the surface layer start to relax. This assumption is based on the several experimental studies. Using the strain measured from LEED I/V as surface strain and the strain averaged from total layers as the volume strain, the Néel type model could explain the SRT behavior of $Co_xNi_{1-x}/Cu_3Au(100)$ with $x \leqslant 11\%$ very well. Besides, the model also can explain the change of MEED period between un-relaxed layer and relaxed layers.

Acknowledgement

This work was supported by National Science Council under grant no. NSC 94-2112-M-002-009 and NSC 94-2112-M-001-045.

References

[1] Néel, Compt. Rend. 237 (1953) 1468;
J. Phys. Radium 15 (1954) 225.
[2] D.P. Pappas, C.R. Brundle, H. Hopster, Phys. Rev. B 45 (1992) 8169.
[3] S. Muller, P. Bayer, C. Reischl, K. Heinz, B. Feldmann, H. Zillgen, M. Wuttig, Phys. Rev. Lett. 74 (1995) 765.
[4] M. Wuttig, B. Feldmann, T. Flores, Surf. Sci. 331–333 (1995) 659.
[5] Minn-Tsong Lin, J. Shen, W. Kuch, H. Jenniches, M. Klaua, C.M. Schneider, J. Kirschner, Surf. Sci. 410 (1998) 290.
[6] F. Baudelet, Minn-Tsong Lin, J. Shen, W. Kuch, H. Jenniches, M. Klaua, C.M. Schneider, J. Kirschner, Phys. Rev. B 51 (1995) 12563.
[7] Minn-Tsong Lin, J. Shen, W. Kuch, H. Jenniches, M. Klaua, C.M. Schneider, J. Kirschner, Phys. Rev. B 55 (1997) 5886.
[8] Minn-Tsong Lin, W.C. Lin, C.C. Kuo, C.L. Chiu, Phys. Rev. B 62 (2000) 14268.
[9] W.C. Lin, C.C. Kuo, C.L. Chiu, Minn-Tsong Lin, Surf. Sci. 478 (2001) 9.
[10] W.C. Lin, C.C. Kuo, C.L. Chiu, Minn-Tsong Lin, J. Appl. Phys. 89 (2001) 7139.
[11] G. Bochi, C.A. Ballentine, H.E. Inglefield, C.V. Thompson, R.C. O'Handley, H.J. Hug, B. Stiefel, A. Moser, H.J. Gunderodt, Phys. Rev. B 52 (1995) 7311.
[12] M. Zheng, J. Shen, P. Ohresser, Ch.V. Mohan, M. Klaua, J. Barthel, J. Kirschner, J. Appl. Phys. 85 (1999) 5060.
[13] G. Bochi, C.A. Ballentine, H.E. Inglefield, C.V. Thompson, R.C. O'Handley, Phys. Rev. B 53 (1996) 1729.
[14] Minn-Tsong Lin, J. Shen, W. Kuch, H. Jenniches, M. Klaua, C.M. Schneider, J. Kirschner, Thin Solid Films 275 (1996) 99.
[15] C. Chappert, P. Bruno, J. Appl. Phys. 64 (1988) 5736.
[16] K. Ha, M. Ciria, R.C. O'Handley, P.W. Stephens, S. Pagola, Phys. Rev. B 60 (1999) 13780.
[17] D. Halley, Y. Samson, A. Marty, P. Bayle-Guillemaud, C. Beigne, B. Gilles, J.E. Mazille, Phys. Rev. B 65 (2002) 205408.
[18] A. Enders, D. Sander, J. Kirschner, J. Appl. Phys. 85 (1999) 5279.
[19] Wei Pan, Dirk Sander, Minn-Tsong Lin, J. Kirschner, Phys. Rev. B 68 (2003) 224419.
[20] W. Pan, R. Popescu, H.L. Meyerheim, D. Sander, O. Robach, S. Ferrer, Minn-Tsong Lin, J. Kirschner, Phys. Rev. B 71 (2005) 174439.
[21] M. Seider, R. Kaltofen, U. Muschiol, Minn-Tsong Lin, C.M. Schneider, J. Appl. Phys. 87 (2000) 5762.
[22] A. Braun, B. Feldmann, M. Wuttig, J. Magn. Magn. Mater. 171 (1997) 16.
[23] M. Henzler, Surf. Sci. 357–358 (1996) 809.
[24] M. Dynna, J.L. Vassent, A. Marty, J. Appl. Phys. 80 (1996) 2650.
[25] J. Shen, J. Giergiel, J. Kirschner, Phys. Rev. B 52 (1995) 8454.
[26] R.F. Willis, J.A.C. Bland, W. Schwarzacher, J. Appl. Phys. 63 (1988) 4051.
[27] W.C. Lin, B.Y. Wang, Y.W. Liao, K.J. Song, Minn-Tsong Lin, Phys. Rev. B 71 (2005) 184413.